Simulations of CO2-CO Infrared Radiation Measurements in Shock and Expansion Tubes

Ulysse Dubuet, Satoshi Nomura, Shingo Matsuyama, Adrien Lemal, Hiroki Takayanagi, Kazuhisa Fujita

Simulations of CO_2-CO Infrared Radiation Measurements in Shock and Expansion Tubes

Ulysse Dubuet*
Paris Saclay University, 91190 Gif-sur-Yvette, France
Satoshi Nomura† and Shingo Matsuyama‡
Japan Aerospace Exploration Agency (JAXA), Tokyo 182-8522, Japan
Adrien Lemal§
ALE Company, Ltd., Tokyo 107-0012, Japan
and
Hiroki Takayanagi¶ and Kazuhisa Fujita**
Japan Aerospace Exploration Agency (JAXA), Institute of Space and Astronautical Science (ISAS), Sagamihara 252-5210, Japan

https://doi.org/10.2514/1.T5853

This Paper presents the simulations of CO_2 and CO infrared radiation behind shock waves and in expansion flows. This work is motivated by the little amount of characterizations of CO_2 infrared radiation in these expansion flows and thermodynamic regimes, whereas carbon dioxide infrared radiation is deemed to contribute significantly to the afterbody heating withstood by a Martian spacecraft. Japan Aerospace Exploration Agency (JAXA) shock-tube facilities were operated at conditions generating flow velocities ranging from 2.8 to 7.3 km/s. Absolute infrared spectra of CO_2 and CO were obtained under equilibrium and nonequilibrium conditions and used to assess the performances of the spectral solvers. Specifically, this Paper introduces the recent enhancements brought to JAXA in-house codes to compute CO_2 nonequilibrium infrared radiation. Schemes to split the level energy into its pure vibrational, rotational, and vibration–rotation coupling and interactions contributions are proposed and implemented. The implementation was evaluated with comparison with literature data and recent measurements. Infrared radiation behind shock waves and under expansion regimes was analyzed with a newly developed model to infer the vibrational and rotational temperatures and determine the degree of thermal nonequilibrium. The latter outlines the highly complicated vibrational energy distribution of carbon dioxide during expansion and the subsequent radiation, as well as the possible shortcomings of the multitemperature models. Therefore, these studies of carbon dioxide nonequilibrium radiation during expansion pose new challenges to the community and will enable the upgrade and validation of the multitemperature and state-to-state models currently in use.

Nomenclature

a, b, c, d	=	powers of coupling temperature $\tilde{T}$
C	=	Wang symmetry quantum number
d	=	CO_2 modal degeneracies
e	=	level energy, J
g	=	level degeneracy
H	=	effective Hamiltonian
h_p	=	Planck constant, equal to $6.62607004 \cdot 10^{-34}$ J · s
J	=	rotational quantum number
k_B	=	Boltzmann constant, equal to $1.38064852 \cdot 10^{-23}$ J/K
l_2	=	magnetic quantum number
N	=	state position in the (P, J, C) block
n_{tot}	=	number density, m^{-3}
n	=	level population, m^{-3}
P	=	polyad quantum number
Q	=	partition function
T	=	temperature, K
v	=	vibrational level

Subscripts

i	=	CO_2 vibrational mode, equal to 1,2,3
R	=	rotation
T	=	translation
V	=	vibration
v_1, v_2, v_3	=	vibrational quantum number of CO_2 vibration modes

Presented as Paper 2019–3015 at the AIAA Aviation Forum, Dallas, Texas, June 17–21, 2019; received 16 July 2019; revision received 18 February 2020; accepted for publication 4 May 2020; published online 11 June 2020.

*Research Assistant, Laboratoire EM2C, CNRS UPR288, CentraleSupélec, 3 rue Joliot Curie; ulysse.dubuet@student.ecp.fr. Member AIAA.

†Researcher, Aeronautical Technology Directorate, Aerodynamic Research Unit, Chofu Aerospace Center, 7-44-1 Jindaiji-Higachi-Machi, Chofu; nomura.satoshi2@jaxa.jp. Member AIAA.

‡Researcher, Aeronautical Technology Directorate, Numerical Simulation Research Unit, Chofu Aerospace Center, 7-44-1 Jindaiji-Higachi-Machi, Chofu; matsuyama.shingo@jaxa.jp. Member AIAA.

§Chief Scientist, 2-11-8 Shibadaimon, Minato-ku, Sumitomo Fudosan Nichome 2F; adrien.lemal@gmail.com. Member AIAA.

¶Researcher, Research and Development Directorate, Research Unit II, Institute of Space and Astronautical Science, 3-1-1 Yoshinodai, Chuo, Sagamihara, Kanagawa 252-5210, Japan; takayanagi.hiroki@jaxa.jp. Member AIAA.

**Professor, Department of Space Flight Systems, Institute of Space and Astronautical Science, 3-1-1 Yoshinodai, Chuo, Sagamihara, Kanagawa 252-5210, Japan; fujita.kazuhisa@jaxa.jp. Senior Member AIAA.

I. Introduction

INTEREST in Mars exploration triggered the development of new missions [1–3], including some based on heritage design [4,5]. Specifically, the design of the front shield has been accomplished through comprehensive numerical simulations and experimental campaigns in shock tubes [6–9] operating at representative flight heating conditions to characterize the convective and radiative heating from the shock layer. The backshell radiative heating, deemed negligible, received little attention until the last decade. The important uncertainties

on the backshell radiation motivated this Paper, which aims to characterize it.

During expansion, the flow undergoes recombination, which can occur under nonequilibrium conditions. Under nonequilibrium conditions, the internal degrees of freedom of CO_2 remain frozen with a significant part of the energy being stored in the vibrational and rotational modes, leading enhanced infrared (IR) radiation [10,11] at 2.3, 2.7, 4.3 and 15 μm. Previous computations also illustrated the dominance of the radiative heating over the convective heating in the afterbody [12–19].

To further characterize the magnitude of this radiation and subsequent radiative heating, experimental campaigns in facilities mimicking expansion processes were undertaken. Japan Aerospace Exploration Agency (JAXA) Chofu Aerospace Centre pioneered the measurement of IR radiation under expansion [20]. Further studies were carried out worldwide to further characterize the possible nonequilibrium state of CO_2 during expansion [21,22]. These original experimental data served as benchmarks to assess the performances of the nonequilibrium flow and spectral models developed in the community [23,24]. The comparison between the simulations and experimental data provided interesting insight on facility artifacts, CO_2 kinetics, and spectral properties but warranted further studies. The flow expansion occurring in the facility was recently characterized, and the thermal state of the flow was inferred from laser absorption techniques [25]. The recent flight measurements onboard the Schiaparelli entry module of the European mission EXOMARS were recently made available to the community [26]. They demonstrated that the radiative heating was dominating over the convective heating. The results from the simulations were compared with the flight data and showed good agreement [27,28]. However, this agreement was not conclusive on the accuracy of the kinetic and spectral model because of the lack of spatial or spectral resolution and limited amount of data.

To strengthen the design of the upcoming missions, modeling improvements and additional measurement campaigns of CO_2 and CO IR radiation behind shock waves and during expansion are warranted. This Paper aims to pursue the experimental campaigns at flight-representative conditions, to measure IR emission spectra at various speed conditions, and to analyze the with JAXA in-house radiative solver.

This Paper is organized into three sections. Section II briefly describes the experimental facility, its sensors, flow, and optical diagnostics used to measure the IR radiation from shocked and expanded flows. Section III describes the computational framework developed to compute the IR radiation. Section IV discusses the results and assesses the performances of the solver by comparing predicted and measured IR spectra for shocked and expansion flows.

II. Experimental Setup

Experimental characterization of the flow surrounding a spacecraft is carried out in high-enthalpy facilities such as shock and expansion tubes. This section briefly presents the Hyper Velocity Expansion Tube (HVET) facility outline and its sensors, as well as its flow and its spatially and spectrally resolved emission spectroscopy diagnostics. More details can be found in [20].

A. Flow Diagnostics

The Hypervelocity Shock-Tube (HVST) facility is a 16 m free-piston driven shock tube consisting of a reservoir tank, a compression tube, a high-pressure tube, a low-pressure tube, a vacuum tank, and a free piston. The expansion of the flow is achieved with the adjunction of an aluminum vacuum chamber. High- and low-pressure tubes are evacuated down to $2 \sim 10$ Pa with a turbomolecular pump and a dry pump before being filled with the gases. Pitot and static pressures were measured with various sensors. For pitot probe measurements, the pressure sensor was mounted in the 25-mm-diam probe inside a 1-mm-diam hole drilled at the tip of the pitot probe. The transducer was protected by a steel disk in order to protect it from the impact of the impurities. The static pressures were measured with two piezoelectric pressure sensors set at 25 and 125 mm upstream from the exit of the expansion section. The rise time of the pressure transducers was lower than 1 μs. The average shock velocity was estimated, given the time elapsed between these transducer measurements. The uncertainties on the pressures and velocities were estimated with the standard deviation of the measured values.

B. Spatially and Spectrally Resolved Optical Diagnostics

Spatial distribution of IR radiation intensity through a magnesium fluoride (MgF_2) window was measured by a 640×512 medium-wavelength IR (MWIR) imager system. The sensor sizes were 24×24 μm. In front of the detector, a high-pass filter was added to reduce the emission from water vapor, which is present near the wall inside the high-pressure, low-pressure tubes and the vacuum chamber.

IR radiation spectra were obtained by the MWIR imager system set behind a Czerny–Turner asymmetric IR spectrometer (Bunkoukeiki Corporation, Ltd., M10-TP). Under shock-tube mode operation, the IR radiation spectra were collected at the position under investigation by an energy optimizer, whereas under expansion-tube mode operation, the IR radiation was collected by a light focus system with a sphere mirror. The entrance slit width was set at 10 μm. The focal length of the monochromator was 170 mm, the spacing between the grooves of the grating was of $2.5 \cdot 10^{-2}$ mm, and the half-angle between the lines joining the center of the grating to the centers of the two mirrors of the monochromator was estimated to be 11 deg. Wavelength calibration was accomplished by measuring the spectrum from a Hg source lamp at a high order of diffraction and by determining the reference wavelength position. The intensity calibration in the IR spectral range was achieved with a blackbody furnace of temperature $T_B = 1673$ K by using the ideal Planck curve. To eliminate the absorption by CO_2 and water vapor from ambient air, the IR spectrometer and the light focus system were purged with N_2 gas. The uncertainties on the radiation measurements were estimated of 30%.

C. Test Conditions

To complement the shock-tube experiments performed in [20], HVST was operated at speed conditions ranging from 2 to 7.5 km $\cdot$ s^{-1} and pressure of 133.3 Pa to fully characterize the radiance withstand by the front shield of a Martian spacecraft along various trajectories. The spectra were integrated along the line of sight perpendicularly to the shock-tube axis to yield the radiance between 4 and 5.4 μm and compared with literature values from NASA Ames Electric Arc Shock Tube (EAST) facility [9], as illustrated in Fig. 1. The differences between the integrated radiance from JAXA HVST and NASA EAST facilities are lower than 30%.

The equilibrium spectral radiances were also compared for lower shock velocities and are shown in Fig. 2. Calibration in the IR spectral range is hindered by the lack of reference lines in this region. Wavelength calibration is achieved by using multiple-order diffracted lines, which essentially yields some calibration errors in wavelength. However, the sensitivity of the sensor does not change with the wavelength, and errors in the absolute radiance are almost constant

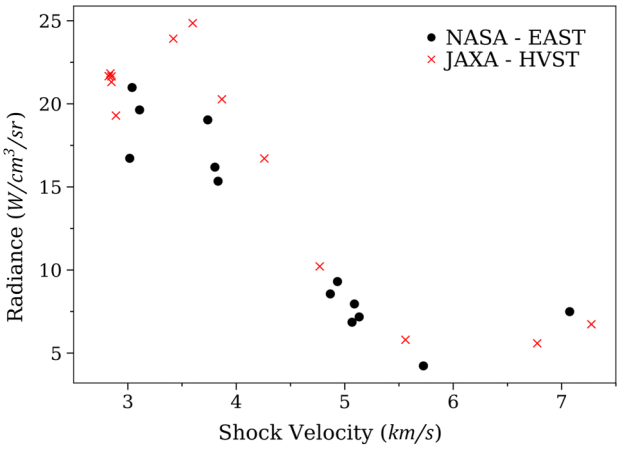

Fig. 1 Equilibrium integrated radiance comparison between JAXA HVST and NASA EAST [9] campaigns, between 4.0 and 5.4 μm.

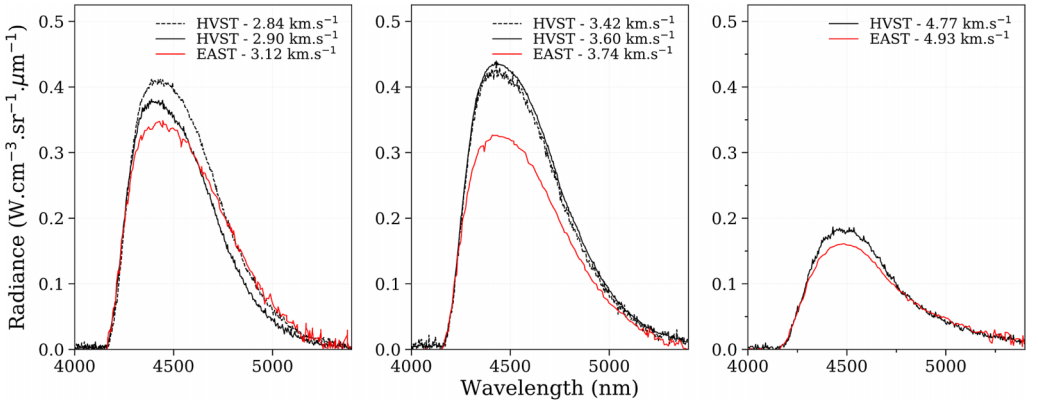

Fig. 2 Comparison of the equilibrium spectral radiance measured in HVST (in black) and EAST (in red) [9] for shock velocities from 2.8 to 5 km · s^{-1}.

and independent of wavelength. Therefore, any small error in the wavelength calibration has little impact on the results of temperature estimation. In the present Paper, the spectra were still shifted by 55 nm in order to match the band heads. Differences lower than 30% are observed between the measured spectra from EAST and HVST facilities for speed ranging from 2.8 to 5 km · s^{-1}, where the radiation is dominated by CO_2. The experimental spectra obtained with HVST for higher shock velocities are shown in Sec. IV.

III. Nonequilibrium Spectral Model

This section describes the multitemperature model for predicting CO_2 IR radiation. JAXA in-house Structured Package for Radiation Analysis (SPRADIAN) code [29] was upgraded [30] to include the Carbon Dioxide Spectroscopic Database (CDSD-4000) [31,32]. The performances of the solver were evaluated by comparing predicted and measured CO_2 IR radiation measurements under a comprehensive set of equilibrium conditions obtained from transmission cells, plasma torches, and shock tubes. CO radiation was previously included [15]. The purpose of the present Paper is to further upgrade the code to simulate nonequilibrium $^{12}C^{16}O_2$ (CO_2 main isotope) IR radiation. The following sections derive the rovibrational levels' energies and present the multitemperature model used for nonequilibrium calculations.

A. Spectral Quantities

Line-by-line emission and absorption coefficients of a transition from an upper level u to a lower level l are computed thanks to Eqs. (1) and (2),

$$\epsilon_{ul}(\lambda) = \frac{h_p c_0 A_{ul}}{4\pi\lambda_{ul}} n_u \Phi(w, \lambda - \lambda_{ul}) \tag{1}$$

$$\alpha_{ul}(\lambda) = \frac{n_l (A_{ul}\lambda_{ul}^4)}{8\pi c_0} \frac{g_u}{g_l}\left[1 - \frac{n_u g_l}{n_l g_u}\right]\Phi(w, \lambda - \lambda_{ul}) \tag{2}$$

where g is the degeneracy of the level (upper or lower). The line centers λ_{ul}, the transition probabilities (Einstein's coefficients) A_{ul}, and the line profile widths w were taken from the CDSD-4000 database [32]. A Voigt line profile Φ as described in [33] is used.

B. Effective Hamiltonian

The present Paper considers the complete expression of the effective Hamiltonian of [31] to compute the rovibrational energy levels. The Hamiltonian is built using the same parameters, and the rovibrational levels' energies are obtained through its diagonalization.

Before diagonalization, it is possible to write the Hamiltonian as a sum of matrices [34], each one corresponding to a dynamic mode, coupling, or interaction, as written in Eq. (3),

$$H_{\text{eff}} = H_{v_1} + H_{v_2} + H_{v_3} + H_{\text{rot}} + \tilde{H} \tag{3}$$

where H_{v_i} corresponds to the ith vibrational mode contribution and $\tilde{H}$ corresponds to the couplings and interactions. The H_{v_i} is composed of the terms using only $(v_i + d_i/2)$ in the diagonal terms of the Hamiltonian, as reminded in Eq. (4):

$$\begin{aligned}(H_{v_i})_{j,j} = \omega_i\left(v_i(j) + \frac{d_i}{2}\right) + x_{ii}\left(v_i(j) + \frac{d_i}{2}\right)^2 \\ + y_{iii}\left(v_i(j) + \frac{d_i}{2}\right)^3 + z_{iiii}\left(v_i(j) + \frac{d_i}{2}\right)^4\end{aligned} \tag{4}$$

To extract the contribution of a particular mode, one must then change the basis of the sub-Hamiltonian written in Eq. (3) to the diagonalization basis. For example, denoting P the diagonalization matrix of the full Hamiltonian (H_{eff}), the mode v_i energy of the state $k = (P, J, C, N)$ is given by Eq. (5):

$$e_{k,v_1} = (P \cdot H_{v_1} \cdot P^{-1})_{k,k} \tag{5}$$

C. Populations

The population of a level $k = (P, J, C, N)$ under thermal nonequilibrium is given by Eq. (6a),

$$n_k = \frac{n_{\text{tot}} g_k}{\tilde{Q}} \exp\left(-\frac{e_{v_1}}{k_B T_{v_1}} - \frac{e_{v_2}}{k_B T_{v_2}} - \frac{e_{v_3}}{k_B T_{v_3}} - \frac{e_{\text{rot}}}{k_B T_{\text{rot}}} - \frac{\tilde{e}}{k_B \tilde{T}}\right) \tag{6a}$$

$$\tilde{Q} = \sum_k g_k \exp\left(-\frac{e_{v_1}}{k_B T_{v_1}} - \frac{e_{v_2}}{k_B T_{v_2}} - \frac{e_{v_3}}{k_B T_{v_3}} - \frac{e_{\text{rot}}}{k_B T_{\text{rot}}} - \frac{\tilde{e}}{k_B \tilde{T}}\right) \tag{6b}$$

$$e_k = e_{v_1} + e_{v_2} + e_{v_3} + e_{\text{rot}} + \tilde{e} \tag{6c}$$

where e_{v_i} is the energy of the ith vibrational mode (as explained in Sec. B), $\tilde{e}$ is the energy of the couplings and different interactions, $\tilde{Q}$ is the nonequilibrium partition function, and $\tilde{T}$ is a coupling temperature.

A database of approximately 7.3 million states has been computed; this corresponds to a maximum polyad number P of 40, a maximum rotational number J of 300, and a cutoff energy of 44600 cm^{-1} corresponding to the dissociation limit of CO_2 626(X).

D. Assessment of Rovibrational Levels

To assess the agreement between our calculated energies and those from CDSD's, simulations of equilibrium spectra (which only depend on the level's energies) around 4.3 μm (approximately 2300 cm^{-1}) were performed at 1000, 2000, and 3000 K with a pressure of 1 atm and 100% of CO_2 and compared with [35]. A rectangular slit function of 10 cm^{-1} has been applied to the spectra. As observed in Fig. 3, a good agreement with the work [35] is observed and gives the authors confidence in the correct computation

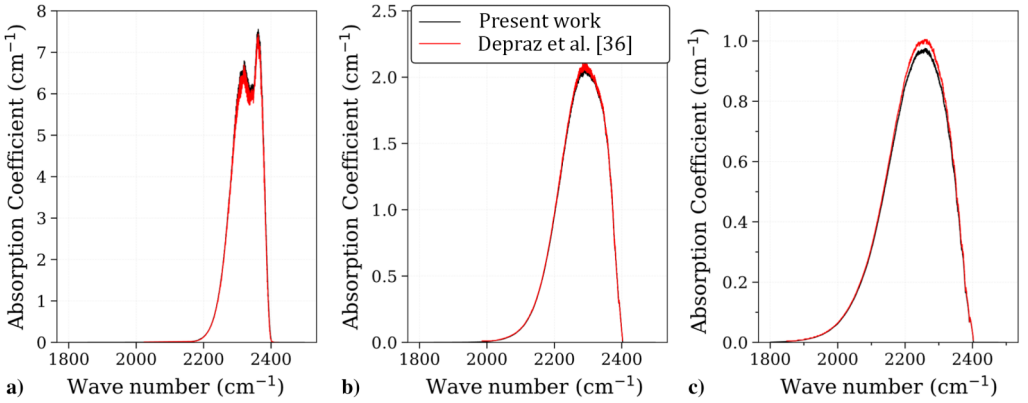

Fig. 3 Comparison of absorption coefficients at equilibrium, with a) $T = 1000$ K, b) $T = 2000$ K, and c) $T = 3000$ K.

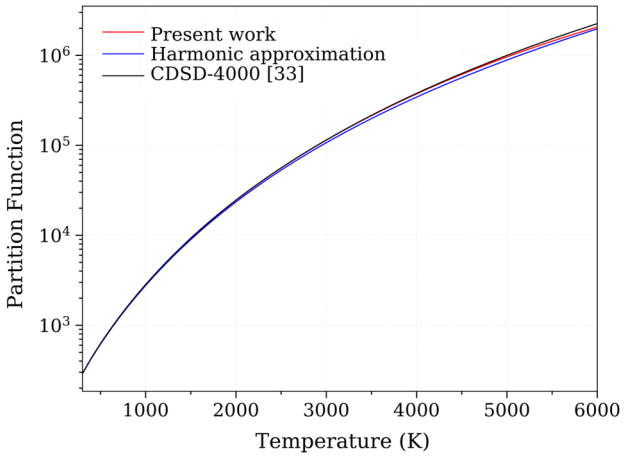

Fig. 4 Comparison of the different partition functions.

of the rovibrational levels' energies and successful upgrade of JAXA SPRADIAN code [29].

Additionally, Fig. 4 shows the comparison between the partition functions computed in this Paper (in red) with CDSD-4000 partition function (in black) and partition function obtained under the harmonic oscillator and rigid rotator approximation [Eq. (7)] (in blue),

$$Q_{\text{Harmonic Approx.}} = \frac{1}{2}\frac{T}{B_e}\left[1-\exp\left(-\frac{\theta_1}{T}\right)\right]^{-1}\left[1-\exp\left(-\frac{\theta_2}{T}\right)\right]^{-2} \times\left[1-\exp\left(-\frac{\theta_3}{T}\right)\right]^{-1} \tag{7}$$

where B_e and $\theta_{j=1,\ldots,3}$ are the spectroscopic constants of the energy term expansion.

The discrepancy with the tabulated partition function is within 0.5% for temperatures up to 3000 K and within 1% for temperatures up to 4300 K. Discrepancies between the computed absorption coefficients become noticeable after $T = 3000$ K, and the relative error between the partition functions is lower than 1% under 4000 K and within 5% under 6000 K, suggesting that the calculation of the higher levels' energies may not be the most accurate and could be improved. Even though the relative error is increasing with the temperature, it is still acceptable for the temperature range of interest, i.e., for temperatures up to 3000 or even 4000 K. The rovibrational levels' energy database will thus be used for the next simulations presented in this Paper.

E. Multitemperature Model

For thermal nonequilibrium CO_2 flow, the choice of the coupling temperature $\tilde{T}$ arises. Inspired by Park's multitemperature model [36], the expression shown in Eq. (8) is proposed. This expression allows us to explore different possibilities and to add the coupling term to any mode or to a combination of the modes,

$$\tilde{T} = T_{v_1}^a T_{v_2}^b T_{v_3}^c T_{\text{rot}}^d \quad \text{where } a+b+c+d=1 \tag{8}$$

F. Effect of Coupling Temperature

To investigate the sensibility to the definition of the coupling temperature, first nonequilibrium simulations were performed. Comparisons were made between absorption and emission spectra with nonequilibrium conditions, for different definitions of the coupling temperature for a pressure of 0.017 atm, 100% of CO_2, and $T_{\text{rot}} = T_{\text{tr}}$. Six different exponent sets were investigated, as detailed in Table 1, with $T_{\text{rot}} = 1700$ K and $T_{v_1} = T_{v_2} = 2100$ K. These temperatures are representative of the possible thermal conditions occurring in the expansion measurements carried out in [20]. The resulting spectra are showed in Fig. 5. They were convoluted with a 10 cm^{-1} square slit function. The different spectral radiances computed are very close to each other. The choice of the definition of the coupling temperature (i.e., the choice of the values of the a, b, c, and d coefficients) does not seem to have a strong impact on the calculated radiance. Other simulations (not shown here) present the same similarities, for temperatures between 1000 and 2000 K. Subsequently, the coupling temperature will be set as $\tilde{T} = \sqrt[3]{T_{v_1}T_{v_2}T_{v_3}}$.

G. Nonequilibrium Transmission Measurements

Nonequilibrium transmission measurements were obtained by Dang et al. [37] and used by [38,39] to infer vibrational temperatures. They found a fit of the transmission data for $T_{\text{rot}} = 491$ K, $T_{v_1} = T_{v_2} = T_{12} = 517$ K, and $T_{v_3} = 2641$ K. The same temperatures were subsequently used to compute the transmittance between 2284.2 and 2284.6 cm^{-1}. The results were compared with the work [38] in Fig. 6. We also compared with RADIS [39] using Boltzmann distributions (Klarenaar et al. [38] use Treanor distributions) and HITRAN [40] database. Good agreement is observed between the various simulations.

Differences between present Paper and [38] may come from the use of different populations distributions and line broadening databases. Work [38] uses a Treanor distribution and HITRAN database [40], while the present Paper uses a Boltzmann distribution and CDSD-4000 [31,32]. The simulation performed with RADIS uses a Boltzmann distribution and HITRAN database and has a very good agreement

Table 1 Coupling temperature definitions studied

Case	a	b	c	d
1	1	0	0	0
2	0	1	0	0
3	0	0	1	0
4	0	0	0	1
5	1/3	1/3	1/3	0
6	1/4	1/4	1/4	1/4

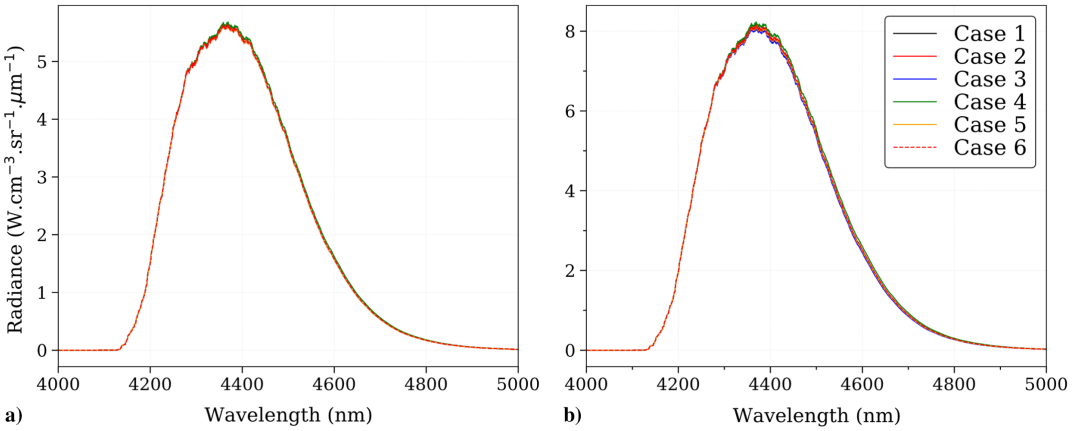

Fig. 5 Influence of the coupling parameters on the radiance with $T_r = 1700$ K, $T_{v_1} = T_{v_2} = 2100$ K and for a) $T_{v_3} = 2100$ K and b) $T_{v_3} = 2600$ K.

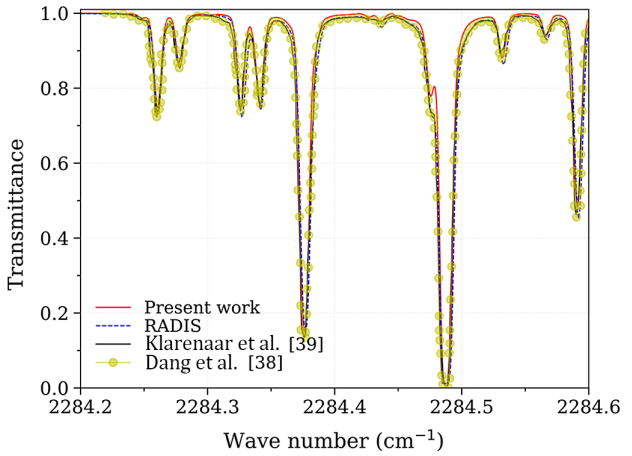

Fig. 6 Comparison between the predicted and measured nonequilibrium CO_2 transmittance spectra.

with the results of Klarenaar [38]. The differences between the present work and Klarenaar's [38] around 2284.7 cm^{-1} can thus be explained by the use of different databases. The present Paper displays two lines easily identifiable, while the latter look partially merged with the HITRAN database.

IV. Results

This section is divided into two parts: first, it presents the measured spectra obtained during the shock-tube measurement campaign and the simulations of these shocked equilibrium flows using the improved radiative solver at equilibrium; second, it presents the analysis of the free-flow previously measured in the expansion-tube HVET [20] by the nonequilibrium features implemented in JAXA radiative solver.

A. Shocked Equilibrium Flows

Radiance was measured in HVST for shock velocities ranging from 2.8 to 7.3 km · s^{-1}. The gas composition and temperatures (for equilibrium and frozen chemistries) were obtained by the code Chemical Equilibrium with Application [41] and are listed in Table 2.

CO radiation was computed using HITEMP database [40], and CO_2 radiation was computed with CDSD-4000 database [31,32] and the updated version of SPRADIAN. The simulated spectra were convoluted by an experimental slit function of full width at half-maximum (FWHM) of 20 nm, able to correctly fit the CO lines for the cases e and f. This is larger than the theoretical value of 5 nm calculated using [42], which is consistent with the theoretical works of [43]. The simulations were compared with the present measurements to highlight the contributions from CO_2 and CO and are shown in Fig. 7.

In this Paper, the plasma was assumed isotropic along the line of sight, and the wall effects and turbulence were neglected. This may induce some discrepancies between simulated and measured spectra, especially for cases a to c.

For shock velocities lower than 5 km · s^{-1}, Figs. 7a and 7b show good agreement between the simulations and the measurements. For these cases, the chemistry is frozen (as the mole fractions of CO_2 are close to 1), and most of the radiation comes from CO_2. For shock velocities greater than 6 km · s^{-1}, Figs. 7e and 7f show good agreement between the simulations and the measurements. For these cases, the chemistry reaches equilibrium because of higher CO_2 dissociation rates. Most of the radiation comes from CO. These results are consistent with [9].

Cases c and d are intermediate conditions and deserve further attention. For case c, reasonable qualitative agreement between simulations and measurements was obtained with CO_2 as the single radiator in the mixture for a pressure $P = 0.518$ bar, a mole fraction $x_{CO_2} = 0.25$, and a temperature of 4500 K. Better agreement with the measurement could be obtained by including the radiation from CO, which would compensate the deficit in radiance after 5 μm. It is thus likely that the mole fraction of CO_2 as well as its temperature are lower than the values presently computed (but larger than at equilibrium), while CO mole fraction is lower than at equilibrium. For case d, the measurement is bounded by simulations with CO_2 radiation (red dashed curve) only and with a hypothetical case 20% CO_2 mixture at $T_{CO_2} = 10\,100$ K (blue curve). For these intermediate cases, the radiance is due to both CO_2 and CO. Further work is warranted on CO_2-CO kinetics, as derived in [44] to improve the prediction of the measured spectra.

B. Expanded Nonequilibrium Flows

This subsection evaluates the performances of the upgraded version of SPRADIAN developed in the present Paper by comparing

Table 2 Simulation parameters

Case	x_{CO_2}	x_{CO}	T_{eq}, K	P, bar
a	1	0	$T_{frozen} = 3350$ K	0.178
b	0.9	0	4000	0.254
c[a]	$1.051 \cdot 10^{-1}$	$5.204 \cdot 10^{-1}$	3400	0.518
c[b]	*0.25*	*0*	*4500*	*0.518*
d[a]	$1.769 \cdot 10^{-2}$	$5.153 \cdot 10^{-1}$	5000	0.693
d[b]	0.2	0	10,100	0.693
e	$6.974 \cdot 10^{-5}$	$4.289 \cdot 10^{-1}$	6500	1.014
f	$4.204 \cdot 10^{-5}$	$3.536 \cdot 10^{-1}$	6900	1.172

[a]The parameters in these lines correspond to the chemical equilibrium for a 4.77 km · s^{-1} and a 5.56 km · s^{-1} shock.
[b]The parameters in these lines correspond to the best fit or upper limit of the experimental radiance.

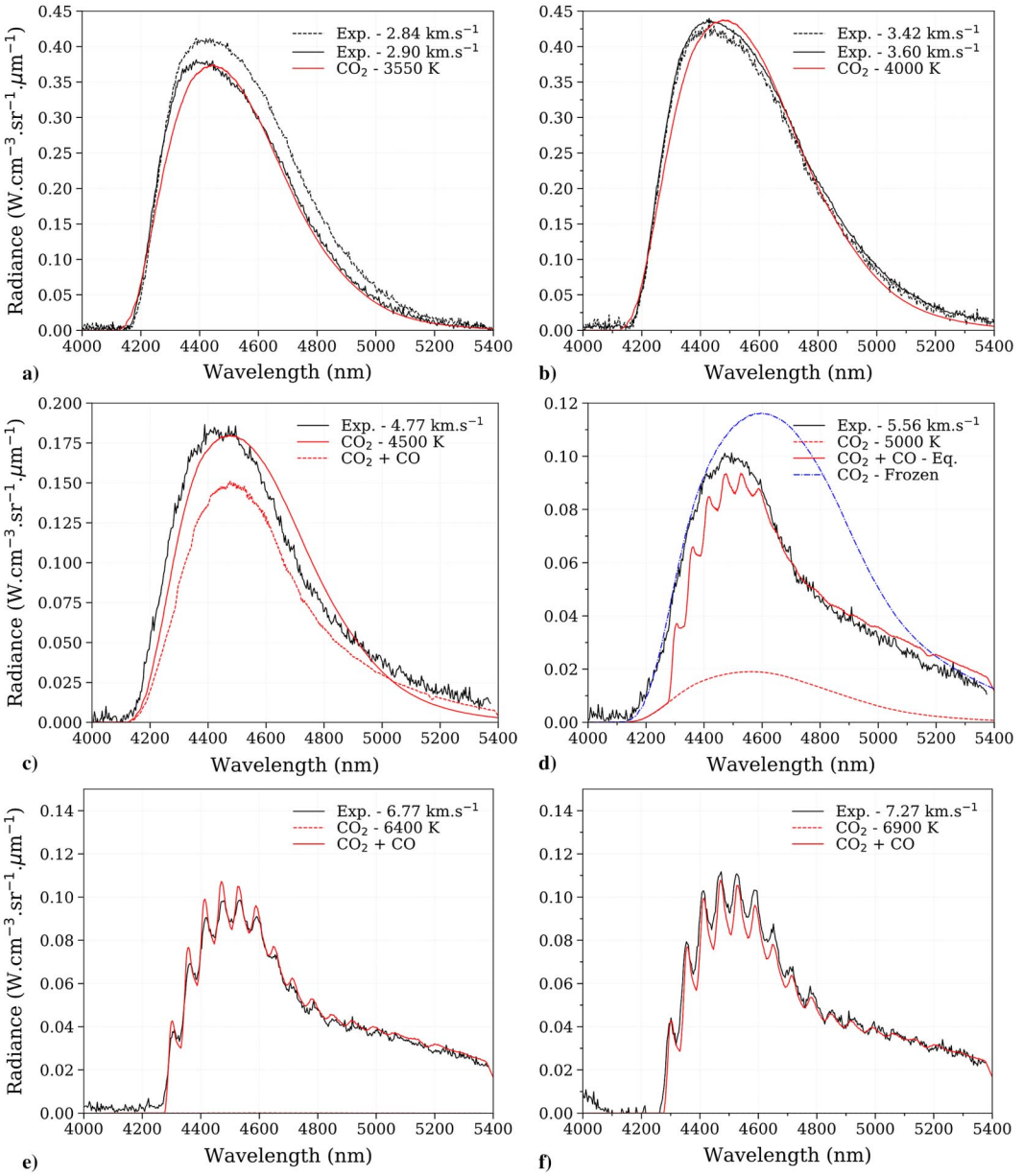

Fig. 7 Comparison between predicted and measured CO_2-CO IR emission spectra. Indices a) to f) correspond to the parameters listed in Table 2.

the simulations with the free-flow measurements (no small-scale sample) of CO_2 IR radiation obtained at JAXA Chofu Aerospace Centre [20]. As stated in the Introduction, these measurements were also used by [23] to assess the performances of the RADIS code [39]. Moreover, this section provides insight on CO_2 vibrational dynamics during expansion and on the degree of nonequilibrium.

Several temperatures and vibrational nonequilibrium simulation conditions were investigated, similarly to the work [23]. CO_2 vibrational dynamics is governed by the relaxation of its three vibrational modes. It is often suggested that the third mode, which is responsible for the emission at 4.3 μm, relaxes more slowly than the first and second modes, which drive the community to assume $T_{v_{12}} \neq T_{v_3}$. This assumption was tested in [23] but was not conducive to significant improvements. Therefore, a two-temperature model, with $T_{v_1} = T_{v_2} = T_{v_3} = T_v$, and $T_{\text{tr}} = T_{\text{rot}}$, was chosen. The simulations were performed for a pressure $p = 1.7 \cdot 10^3$ Pa and a CO_2 mole fraction $x_{CO_2} = 0.61$ (i.e. the same parameters used in [20] for the adjusted Park's two-temperature model).

The evaluation of SPRADIAN's accuracy was accomplished in two steps: 1) predicting the band head around 4.2 μm and 2) predicting the tail of the curve. To predict the band head, the rotational temperature was first determined assuming rovibrational equilibrium; then, the various vibrational temperatures and degree of nonequilibrium were adjusted to match the measurement. The comparison between the measurement and the various simulations is displayed in Fig. 8. This approach led to $T_r = 1700$ K and $T_v = 2100$ K, which compare favorably with the temperatures determined in [23] ($T_r = 1700$ K and $T_v = 2200$ K). The spectral shape being very sensitive to the temperature, a slight change of the temperature quickly changes the entire shape of the spectrum, which confirms that our estimation of a 100 K error in temperature estimation is not underestimated. Figure 8 shows that SPRADIAN agrees better with the experimental value than RADIS [23,39]. Of noticeable importance, the vibrational temperature is twice smaller than the one predicted by Park's two-temperature model (4000 K) [20,36]. The vibrational modes would thus relax quicker than the two-temperature model predictions, which requires an update of the Park model [36] for CO_2-based flows.

From Fig. 8, discrepancies remain between the simulations and the measurements after 4.6 μm, the simulated radiance being lower than the measured one. Possible reasons could be the contribution to CO radiation or a non-Boltzmann distribution of the levels emitting at this spectral range. Considering a collisional-radiative model such as

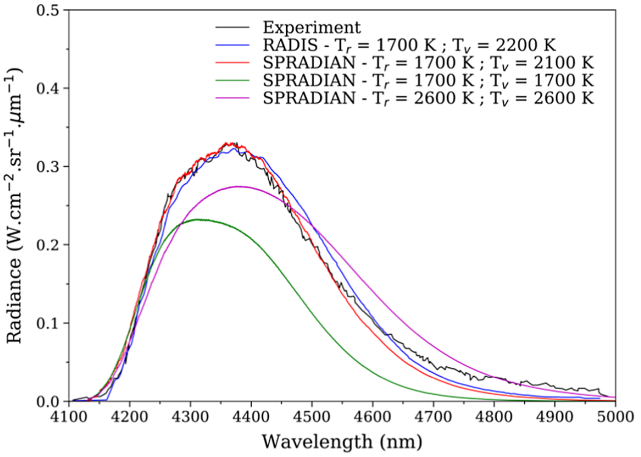

Fig. 8 Comparison of measurements in HVET and simulated nonequilibrium CO_2 radiance during expansion (free flow). Fit with RADIS [23] (in blue) is also displayed.

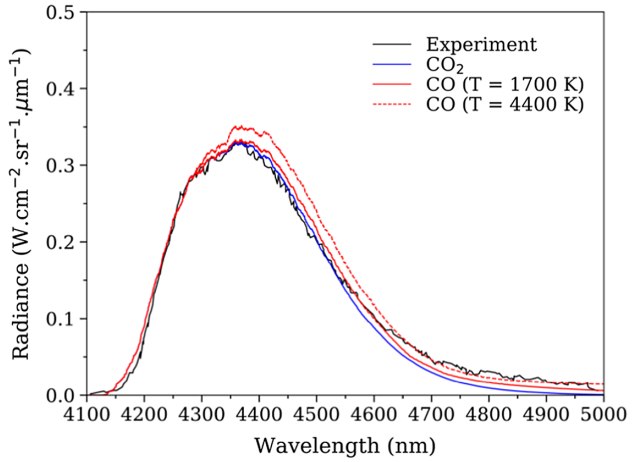

Fig. 9 Comparison of the measured radiance and the simulated spectra, including the contribution of CO for $T_{CO} = 1700$ K or $T_{CO} = 4400$ K.

developed in [45] is beyond the scope of the present Paper. Thus, the contribution of CO in the radiation was investigated, and the results are displayed in Fig. 9. For a CO-temperature of 4400 K, there is good agreement between 4.6 and 5 μm, but the radiance between 4.3 and 4.6 μm is overestimated, and the residual is higher than when CO_2 is solely considered. Various CO temperatures ranging from 1700 to 4400 K were then considered. The resulting spectra were compared with the simulation with only CO_2. The minimum discrepancy with the measurement were achieved for $T_{CO} = 1700$ K, which, however, does not mitigate the discrepancies between the predicted at measured radiances after 4.6 μm. Future work is therefore required.

V. Conclusions

This Paper presents new measurements performed at JAXA HVST, the improvements to JAXA in-house radiation solver to compute CO_2 IR radiation under thermal nonequilibrium, and its application to the shock- and expansion-tube measurements.

The measurements made with HVST were performed to expand the experimental data regarding CO_2 IR radiation in shocked conditions and to further validate the modeling tools. JAXA shock-tube facilities were operated at conditions generating flow velocities ranging from 2.8 to 7.3 km $\cdot$ s^{-1}. Absolute spectral measurements were obtained in the 4.3 μm region and integrated to yield absolute radiances. The latter were compared to the measurements obtained at NASA EAST facility, and good agreement was obtained.

The improvements to JAXA in-house solver now include the contributions of the couplings and interactions in the computation of CO_2 energy levels. An accurate computation of the energy levels was also undertaken, and good agreement was achieved between our work and the simulations in the literature. Thermal nonequilibrium was described under the multitemperature formalism, with the definition of a coupling temperature. The model results were then compared with experimental and simulation results under the nonequilibrium conditions of a CO_2 laser discharge. Excellent agreement was obtained between the present simulations and the measured transmission spectra.

Once the model was validated, it was used to analyze JAXA shock-tube measurements. It confirmed EAST observations: for shock velocities greater than 5 km $\cdot$ s^{-1}, the flow reaches chemical equilibrium, and CO IR radiation dominates CO_2 radiation. For the low- and high-speed conditions, good agreement was obtained between the simulations and the measured spectra. The experimental expansion-tube spectra previously measured were analyzed with the present nonequilibrium model to determine the vibrational and rotational temperatures as well as the degree of nonequilibrium. Specifically, the measurements obtained during expansion confirms the nonequilibrium between vibrational and rotational temperatures. The relaxation times were found faster from the predictions using the Park two-temperatures model.

Acknowledgments

Thanks are due to C. O. Laux and E. Pannier (EM2C laboratory, CentraleSupélec, France) for their advice on the calculation of CO_2 rovibrational energies. The improvements of the radiative solver were made thanks to a collaboration agreement between National Center for Scientific Research and Japan Aerospace Exploration Agency (JAXA). Thanks are due to Japan Aerospace Exploration Agency (JAXA) and EM2C/National Center for Scientific Research administrative staff for making this agreement possible.

References

[1] Hwang, H., Bose, D., Wright, H., White, T. R., Schoenenberger, M., Santos, J., Karlgaard, C. D., Kuhl, C., Oishi, T., and Trombetta, D., "Mars 2020 Entry, Descent, and Landing Instrumentation (MEDLI2)," *46th AIAA Thermophysics Conference*, AIAA Paper 2016-3526, 2016.

[2] Bayle, O., Portigliotti, S., Venditto, P., Walpot, L., Beck, J. C., Tran, P., and Guelhan, A., "ExoMars 2016 Descent Module EDL Demonstration Mission. Approach to Aerodynamic and Aerothermodynamic Database Building," *Proceedings of '7th International Symposium on Aerothermodynamics for Space Vehicles*, ESA SP-692, Brugge, Belgium, May 2011, p. 2.

[3] Fujita, K., Hatakenaka, R., Nishi, K., Ikenaga, T., Suzuki, T., Haruki, M., Ozawa, T., Nomura, S., Usui, T., Miyamoto, H., and Kameda, S., "Conceptual Study of Mars Aerocapture Orbiter for Engineering Observation and Science Observation," *32nd ISTS and 9th NSAT Conference*, 2019-k-57, Fukui, Japan, June 2019, pp. 1–7.

[4] Edquist, K., Wright, M., and Allen, G., "Viking Afterbody Heating Computations and Comparisons to Flight Data," AIAA Paper 2006-0386, 2006.

[5] Edquist, K., Dyakonov, A., Wright, M., and Tang, C., "Aerothermodynamic Environments Definition for the Mars Science Laboratory Entry Capsule," AIAA Paper 2007-1206, 2006.

[6] Takayanagi, H., and Fujita, K., "Infrared Radiation Measurement Behind Shock Wave in Mars Simulant Gas for Aerocapture Missions," *44th AIAA Thermophysics Conference*, AIAA Paper 2013-2504, 2013.

[7] Brandis, A. M., Johnston, C. O., Cruden, B. A., Prabhu, D. K., Wray, A. A., Liu, Y., Schwenke, D. W., and Bose, D., "Validation of CO 4th Positive Radiation for Mars Entry," *Journal of Quantitative Spectroscopy and Radiative Transfer*, Vol. 121, May 2013, pp. 91–104. https://doi.org/10.1016/j.jqsrt.2013.02.009

[8] Johnston, C. O., and Brandis, A. M., "Modeling of Nonequilibrium CO Fourth-Positive and CN Violet Emission in $CO_2 - N_2$ Gases," *Journal of Quantitative Spectroscopy and Radiative Transfer*, Vol. 149, Dec. 2014, pp. 303–317. https://doi.org/10.1016/j.jqsrt.2014.08.025.

[9] Cruden, B. A., Brandis, A. M., and Prabhu, D. K., "Measurement and Characterization of Mid-Wave Infrared Radiation in CO_2 Shocks," *11th AIAA/ASME Joint Thermophysics and Heat Transfer Conference*, AIAA Paper 2014-2962, 2014.

[10] Sundberg, R., Duff, J., and Bernstein, L., "Nonequilibrium Infrared Emission Model for Reentry Vehicles," *27th AIAA Thermophysics Conference*, AIAA Paper 1992-2916, 1992.

[11] Binauld, Q., Rivière, P., Lamet, J.-M., Tessé, L., and Soufiani, A., "CO_2 IR Radiation Modelling with a Multi-Temperature Approach in Flows Under Vibrational Nonequilibrium," *Journal of Quantitative Spectroscopy and Radiative Transfer*, Vol. 239, Dec. 2019, Paper 106652. https://doi.org/10.1016/j.jqsrt.2019.106652

[12] Rouzaud, O., Tesse, L., Soubrie, T., Soufiani, A., Riviere, P., and Zeitoun, D., "Influence of Radiative Heating on a Martian Orbiter," *Journal of Thermophysics and Heat Transfer*, Vol. 22, No. 1, 2008, pp. 10–19. https://doi.org/10.2514/1.28259

[13] Lino Da Silva, M., and Beck, J., "Contribution of CO_2 IR Radiation to Martian Entries Radiative Wall Fluxes," *49th AIAA Aerospace Sciences Meeting*, AIAA Paper 2011-0135, 2011.

[14] Surzhikov, S., and Omaly, P., "Radiative Gas Dynamics of Martian Space Vehicles," *49th AIAA Aerospace Sciences Meeting*, AIAA Paper 2011-0452, 2011.

[15] Fujita, K., Matsuyama, S., and Suzuki, T., "Prediction of Forebody and Aftbody Heat Transfer Rate for Mars Aerocapture Demonstrator," AIAA Paper 2012-3001, 2012.

[16] Brandis, A. M., Cruden, B. A., White, T. R., Saunders, D. A., and Johnston, C. O., "Radiative Heating on the After-Body of Martian Entry Vehicles," *45th AIAA Thermophysics Conference*, AIAA Paper 2015-3111, 2015.

[17] Potter, D. F., Karl, S., Lambert, M., and Hannemann, K., "Computation of Radiative and Convective Contributions to Viking Afterbody Heating," *44th AIAA Thermophysics Conference*, AIAA Paper 2013-2095, 2013.

[18] Edquist, K. T., Hollis, B. R., Johnston, C. O., Bose, D., White, T. R., and Mahzari, M., "Mars Science Laboratory Heat Shield Aerothermodynamics: Design and Reconstruction," *Journal of Spacecraft and Rockets*, Vol. 51, No. 4, 2014, pp. 1106–1124. https://doi.org/10.2514/1.A32749

[19] West, T. K., Theisinger, J., Brune, A. J., and Johnston, C. O., "Backshell Radiative Heating on Human-Scale Mars Entry Vehicles," AIAA Paper 2017-4532, 2017.

[20] Takayanagi, H., Lemal, A., Nomura, S., and Fujita, K., "Measurements of Carbon Dioxide Nonequilibrium Infrared Radiation in Shocked and Expanded Flows," *Journal of Thermophysics and Heat Transfer*, Vol. 32, No. 2, 2018, pp. 483–494. https://doi.org/10.2514/1.T5200

[21] Gu, S., "Mars Entry Afterbody Radiative Heating: An Experimental Study of Nonequilibrium CO_2 Expanding Flow," Ph.D. Thesis, The Univ. of Queensland, Brisbane, Australia, 2017.

[22] Leibowitz, M. G., and Austin, J. M., "Hypervelocity Measurements of Mid-Wave Infrared CO_2 Radiation Impinging on Blunt Bodies," *AIAA Scitech 2019 Forum*, AIAA Paper 2019-1555, Jan. 2019, pp. 1–13. https://doi.org/10.2514/6.2019-1555

[23] Pannier, E., and Laux, C. O., "Analysis of the JAXA Nonequilibrium Infrared Emission Spectra for Mars Entry Conditions," *Journal of Thermophysics and Heat Transfer*, Vol. 33, No. 4, 2019, pp. 1127–1131. https://doi.org/10.2514/1.T5646

[24] Dubuet, U., Lemal, A., Nomura, S., Takayanagi, H., Matsuyama, S., and Fujita, K., "Simulations of CO_2-CO Infrared Radiation Measurements in Shock and Expansion-Tubes," *AIAA SciTech 2019 Forum*, AIAA Paper 2019-3015, 2019.

[25] Nomura, S., and Fujita, K., "Translational Temperature Measurements of CO_2 Flow in Expansion Tube," *International Conference on Flight Vehicles, Aerothermodynamics, Reentry Missions and Engineering*, Monopoli, Italy, Sept.–Oct. 2019.

[26] Gülhan, A., Thiele, T., Siebe, F., Kronen, R., and Schleutker, T., "Aerothermal Measurements from the ExoMars Schiaparelli Capsule Entry," *Journal of Spacecraft and Rockets*, Vol. 56, No. 1, 2019, pp. 68–81. https://doi.org/10.2514/1.A34228

[27] Annaloro, J., Boubert, P., Bultel, A., Druguet, M., Duffour, E., Jacquot, M., Lago, V., Menecier, S., Perisse, F., Rembaut, N., Riviere, P., Soufiani, A., Martin, S., and Vacher, D., "Rebuilding of ICOTOM Radiometer Data During the Schiaparelli Martian Entry," *8th International Workshop on Radiation of High Temperature Gases for Space Missions*, Madrid, Spain, March 2019.

[28] Brandis, A. M., White, T. R., Saunders, D., Hill, J., and Johnston, C. O., "Simulation of the Schiaparelli Entry and Comparison to Aerothermal Flight Data," *AIAA Aviation 2019 Forum*, AIAA Paper 2019-3260, 2019.

[29] Fujita, K., and Abe, T., "SPRADIAN, Structured Package for Radiation Analysis: Theory and Application," Inst. of Space and Astronautical Science Rept. 669, Sagamihara, Kanagawa, Japan, 1997, pp. 50–97.

[30] Lemal, A., Takayanagi, H., Nomura, S., and Fujita, K., "Simulations of Carbon-Dioxide Equilibrium Infrared Radiation Measurements," *Journal of Thermophysics and Heat Transfer*, Vol. 32, No. 1, 2018, pp. 184–195. https://doi.org/10.2514/1.T5134

[31] Tashkun, S. A., Perevalov, V. I., Teffo, J. L., Rothman, L. S., and Tyuterev, V. G., "Global Fitting of $^{12}C^{16}O_2$ Vibrational-Rotational Line Positions Using the Effective Hamiltonian Approach," *Journal of Quantitative Spectroscopy and Radiative Transfer*, Vol. 60, No. 5, 1998, pp. 785–801. https://doi.org/10.1016/S0022-4073(98)00082-X

[32] Tashkun, S. A., and Perevalov, V. I., "CDSD-4000: High-Resolution, High-Temperature Carbon Dioxide Spectroscopic Databank," *Journal of Quantitative Spectroscopy and Radiative Transfer*, Vol. 112, No. 9, 2011, pp. 1403–1410. https://doi.org/10.1016/j.jqsrt.2011.03.005

[33] Whiting, E. E., "An Empirical Approximation to the Voigt Profile," *Journal of Quantitative Spectroscopy and Radiative Transfer*, Vol. 8, No. 6, 1968, pp. 1379–1384. https://doi.org/10.1016/0022-4073(68)90081-2

[34] Pannier, E., "Conversion of Carbon Dioxide with Nanosecond Pulsed Discharges," Ph.D. Thesis, CentraleSupélec, Gif-sur-Yvette, France, 2019.

[35] Depraz, S., "Etude Expérimentale et Modélisation des Propriétés Radiatives des Mélanges Gazeux de Type $CO_2 - N_2$ à Très Haute Température en Vue de l'application aux Rentrées Atmosphériques Martiennes," Ph.D. Thesis, Ecole Centrale Paris, Châtenay-Malabry, France, 2011, p. 136 (in French).

[36] Park, C., Howe, J. T., Jaffe, R. L., and Candler, G. V., "Review of Chemical-Kinetic Problems of Future NASA Missions II- Mars Entries," *Journal of Thermophysics and Heat Transfer*, Vol. 8, No. 1, 1994, pp. 1–14.

[37] Dang, C., Reid, J., and Garside, B. K., "Detailed Vibrational Population Distributions in a CO_2 Laser Discharge as Measured with a Tunable Diode Laser," *Applied Physics B Photophysics and Laser Chemistry*, Vol. 27, No. 3, 1982, pp. 145–151. https://doi.org/10.1007/BF00694640

[38] Klarenaar, B. L. M., Engeln, R., van den Bekerom, D. C. M., van de Sanden, M. C. M., Morillo-Candas, A. S., and Guaitella, O., "Time Evolution of Vibrational Temperatures in a CO_2 Glow Discharge Measured with Infrared Absorption Spectroscopy," *Plasma Sources Science and Technology*, Vol. 26, No. 11, 2017, Paper 115008. https://doi.org/10.1088/1361-6595/aa902e

[39] Pannier, E., and Laux, C. O., "RADIS: A Nonequilibrium Line-by-Line Radiative Code for CO_2 and HITRAN-Like Database Species," *Journal of Quantitative Spectroscopy and Radiative Transfer*, Vols. 222–223, Jan. 2019, pp. 12–25. https://doi.org/10.1016/j.jqsrt.2018.09.027

[40] Rothman, L. S., Gordon, I. E., Barber, R. J., Dothe, H., Gamache, R. R., Goldman, A., Perevalov, V. I., Tashkun, S. A., and Tennyson, J., "HITEMP, the High-Temperature Molecular Spectroscopic Database," *Journal of Quantitative Spectroscopy and Radiative Transfer*, Vol. 111, No. 15, 2010, pp. 2139–2150. https://doi.org/10.1016/j.jqsrt.2010.05.001

[41] McBride, B. J., and Gordon, S., "Computer Program for Calculation of Complex Chemical Equilibrium Compositions and Applications," NASA Reference Publication 1311, 1996.

[42] Laux, C., Gessman, R., Hilbert, B., and Kruger, C., "Experimental Study and Modeling of Infrared Air Plasma Radiation," AIAA Paper 1995-2124, 1995.

[43] Lerner, J. M., and Thevenon, A., *The Optics of Spectroscopy*, Tutorial, Massachusetts Inst. of Technology, Cambridge, MA, 1975.

[44] Cruden, B. A., Brandis, A. M., and Prabhu, D. K., "Compositional Dependence of Radiance in $CO_2/N_2/Ar$ Systems," *44th AIAA Thermophysics Conference*, AIAA Paper 2013-2502, 2013.

[45] Sahai, A., Johnston, C. O., Lopez, B., and Panesi, M., "Flow-Radiation Coupling in CO_2 Hypersonic Wakes Using Reduced-Order Non-Boltzmann Models," *Physical Review Fluids*, Vol. 4, No. 9, 2019, Paper 093401. https://doi.org/10.1103/PhysRevFluids.4.093401

[46] Cruden, B. A., Brandis, A. M., and Prabhu, D. K., "Measurement and Characterization of Mid-Wave Infrared Radiation in CO_2 Shocks," *11th AIAA/ASME Joint Thermophysics and Heat Transfer Conference*, AIAA Paper 2014-2962, 2014.